Korean J. Chem. Eng., 39(3), 548-561 (2022)
DOI: 10.1007/s11814-021-0954-6

pISSN: 0256-1115
eISSN: 1975-7220

Effect of nonlinear drag on the onset and the growth of the miscible viscous fingering in a porous medium

Min Chan Kim†

Department of Chemical Engineering, Jeju National University, Jeju 63243, Korea
(*Received 5 July 2021 • Revised 20 August 2021 • Accepted 5 September 2021*)

Abstract−The onset and growth of miscible viscous fingering in a porous medium was analyzed analytically. Taking the nonlinear drag into account, new stability equations were derived based on Forchheimer's extension and solved with the quasi-steady state approximation in a similar domain (QSSAξ). Also, the validity of QSSAξ was tested by the numerical initial value calculation (IVC) study. Through the initial growth rate analysis without the steady state approximation, we showed that initially the system is unconditionally stable even in unfavorable viscosity distribution and there exists an initial condition with the largest growth rate. The present initial growth rate analysis without the QSSA is quite different from the previous analyses based on quasi-steady state approximation in the global domain (QSSAx), where the system is assumed to be unstable if the less viscosity fluid displaces the higher one. Employing the linear stability results as an initial condition, fully non-linear numerical simulations were conducted using the Fourier spectral method. The present linear and non-linear analyses predicted that the non-linear drag makes the system stable, i.e., it delays the onset of instability and suppresses the evolution of fingering motions.

Keywords: Viscous Fingering, Non-linear Drag, Forchheimer's Extension, Linear Stability Analysis, Non-linear Numerical Simulation

INTRODUCTION

When a less viscous fluid displaces another miscible more viscous fluid, *i.e.*, viscosity increases along the main flow direction, a secondary motion called miscible viscous fingering (VF) deforms parallel viscosity contours into fingerlike patterns. Hill [1] first studied the instability during the displacement of two-miscible fluids in a porous medium to understand a channeling which sometimes occurs when one fluid follows another along a uniformly packed column. VF in a porous medium is an important issue in many engineering fields, such as enhanced oil recovery, pollution spreading in soils, chromatographic column design, and so on [2,3]. To understand the onset and evolution of VF, many researchers have studied it theoretically and experimentally.

Slobod and Thomas [4] systematically analyzed the onset and the evolution of the miscible VF by employing X-ray visualization. According to their experimental results, there exist a stable region even for the system having unfavorable viscosity distribution, and the stability characteristics, such as the onset position and the wavelength of VF instability, are influenced by the viscosity distribution and also, the flow rate. Further evidence of fingering has been reported by using the nuclear magnetic resonance (NMR) imaging technique [5], the optical method [6], and the echo-planar spectroscopic imaging method [7]. To explain Slobod and Thomas's [4] experiment, based on the quasi-steady state approximation (here, called QSSAx), Tan and Homsy [5] suggested theoretically that the unfavorable viscosity distribution makes the system unconditionally unstable and induces VF instability. In addition, Tan and Homsy [8] solved the same problem using an initial value calculation (IVC) method to support their QSSAx results. Unlike their QSSA, Tan and Homsy [8] IVC reveal that the disturbances under the unfavorable viscosity distribution have large negative growth rate during the early stage of displacing.

Later, Pramanik and Mishra [9-12] considered the effects of the Korteweg stress on the onset of the viscous fingering using a quasi-steady-state-approximation in the self-similar domain (QSSAξ). According to their linear and nonlinear stability analyses results, the QSSAξ can relax the discrepancy between the previous QSSAx and the IVC. Recently, by employing non-modal analysis (NMA), Hota and Mishra [13] revisited the effect of non-monotonic viscosity on the onset of VF of miscible displacement in porous media. Their NMA results show that the non-monotonic viscosity-concentration profile has a significant influence on the onset of instability and the shape of eigenfunctions. In addition, the effects of shear thinning on the onset and the growth of miscible viscous fingering instabilities have been analyzed by Kim and Choi [14], and Shoghi and Norouzi [15]. They showed that a flow where displacing fluid is a shear-thinning is always more unstable than the Newtonian counterpart. However, when a Newtonian fluid displaces a shear-thinning one, the shear-thinning effect in general makes the system stable. Norouzi et al. [16] analyzed the effect of viscous dissipation on the growth of VF in a porous medium. According to their numerical simulation, the viscous dissipation makes the system stable and, therefore, it impedes the development of the VF motion.

For a flow in a Hele-Shaw cell, Yuan and Azaiez [17,18] analyzed

†To whom correspondence should be addressed.
E-mail: mckim@cheju.ac.kr

the inertia effect on the onset of viscous fingering by adding the acceleration and inertia terms to the Darcy's model. According to their analysis, the additional effects make the systems stable, *i.e.*, they retard the onset of instability motions. However, as pointed by Beck [19], even though their inertia term, $\beta\mathbf{u}\cdot\nabla\mathbf{u}$, can explain the inertia effect in a Hele-Shaw cell, it is inappropriate for the nonlinear drag in a porous medium because it is identically zero for steady incompressible unidirectional flow no matter how large the fluid velocity. For the buoyancy-driven instability in a porous medium, Chung et al. [20] showed that the non-linear drag and dispersion effects retard the onset and the growth of instability motion. Therefore, the effect of non-linear drag on the onset and growth of miscible VF instability in a porous medium should be analyzed using a more reliable flow model.

In the present study, the effect of nonlinear drag on the onset condition of VF was analyzed using linear stability theory and nonlinear numerical simulations. By adopting Forchheimer's extension as a flow model, new stability equations were derived and solved analytically and numerically with and without the quasi-steady state approximation. Also, we show that for the extreme case of small time or small displacing velocity, the system is unconditionally stable even in unfavorable viscosity distribution and there exists a least stable initial condition. Using this least stable initial condition as a starting point, the effect of nonlinear drag on the growth of the viscous fingering instabilities was analyzed through the fully nonlinear numerical simulations. The present linear and nonlinear studies are in good agreement.

GOVERNING EQUATIONS AND BASE FIELDS

In a fluid-saturated porous medium, if one Newtonian incompressible fluid displaces another miscible one with the uniform velocity U_0, as schematized in Fig. 1, the governing equations consist of continuity, momentum and mass transport equations in a reference frame moving with the injection velocity U_0 can be expressed as [21]:

$$\nabla\cdot\mathbf{U}=0, \tag{1}$$

$$\nabla P=-\left\{\frac{\mu(C)}{K}+\beta_F\rho|\mathbf{i}U_0+\mathbf{U}|\right\}(\mathbf{i}U_0+\mathbf{U}), \tag{2}$$

$$\frac{\partial C}{\partial t}+\mathbf{U}\cdot\nabla C=\nabla\cdot(\mathbf{D}\cdot\nabla C), \tag{3}$$

under the following initial and boundary conditions:

$$C(X,0)=C_+ \text{ for } X>0 \text{ and } C(X,0)=C_- \text{ for } X\le 0, \tag{4a}$$

$$\mathbf{U}(X,t)\to\mathbf{0} \text{ as } \mathbf{X}\to\pm\infty, \tag{4b}$$

$$P(X,t)\to P_- \text{ as } X\to-\infty, \tag{4c}$$

$$C(X,t)\to C_+ \text{ as } X\to\infty \text{ and } C(X,t)=C_- \text{ as } X\to-\infty, \tag{4d}$$

where, $\mathbf{U}\{=(U,V,W)\}$ is the velocity vector in the Cartesian coordinate $\mathbf{X}\{=(X,Y,Z)\}$, P the pressure, $\mu(C)$ the concentration dependent viscosity, K the constant permeability, β_F the Forchheimer constant, ρ the density of fluid, $\mathbf{i}$ the unit vector along the main flow direction, t the time, and C the concentration. Here P_- is an arbitrary reference pressure. It should be kept in mind that the time derivative in Eq. (3) is the time derivative in a reference frame moving with unidirectional velocity $\mathbf{i}U_0$. For the present unidirectional flow, the dispersion tensor $\mathbf{D}$ has been expressed as

$$\mathbf{D}=\begin{bmatrix} D_L & 0 & 0\\ 0 & D_T & 0\\ 0 & 0 & D_T\end{bmatrix}, \tag{5}$$

where D_L and D_T are the streamwise and spanwise dispersion coefficients, respectively.

In practice, by setting $\beta_F=0$ in Eq. (2), Darcy's equation can applied for the system of $Re_p<1$; here $Re_p(=\rho U_0 d_p/\mu)$ is the Reynolds number based on the particle diameter d_p [22]. As the injection velocity, U_0, increases, a smooth transition to the nonlinear drag region has been observed for $1<Re_p<10$ [21]. According to Joseph et al. [23], Eq. (2) is the appropriate modification Darcy's model, and is known as Forchheimer's extension. The Forchheimer term, the second term of the right hand side of Eq. (2), is included to explain nonlinear drag for the region of $1<Re_p<10$. For a non-spherical porous matrix, $Re_K(=\rho U_0 c_F\sqrt{K}/\mu)$ which uses $\sqrt{K}$ as a length scale is more general parameter, and Forchheimer's extension (2) has been applied for $Re_K<10^2$ [24]. Here, $c_F(=\beta_F\sqrt{K})$ is the dimensionless form drag coefficient.

Note that the inertia term in a viscous fluid, $(\mathbf{i}U_0+\mathbf{U})\cdot\nabla\mathbf{U}$, is not included in Eq. (2). Nield and Bejan [20] clearly explained that unlike a viscous fluid layer, in a porous medium the Forchheimer term is much more important than the inertia term, $(\mathbf{i}U_0+\mathbf{U})\cdot\nabla\mathbf{U}$. Furthermore, as discussed by Beck [19], Forchheimer's extension does not increase the order of differential equation and can be consistent with the slip boundary condition, which is appropriate for Darcy's equation. Based on these physical and mathematical advantages, we employed Forchheimer's extension as a momentum equation.

Considering the characteristic length, $D_L/(RU_0)$, and time, $D_L/$

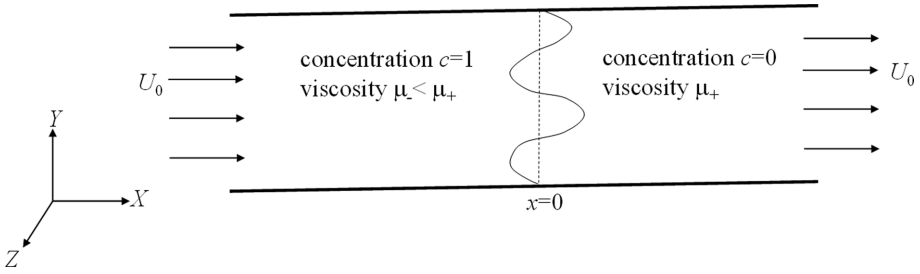

Fig. 1. Schematic diagram of the system considered here.

$(RU_0)^2$, the dimensionless governing equations are expressed as

$$\nabla\cdot\mathbf{u}=0, \tag{6}$$

$$\nabla p=-(\bar{\mu}+Re_K ND)\left(\frac{\mathbf{i}}{R}+\mathbf{u}\right), \tag{7a}$$

$$ND=\sqrt{1+2R\mathbf{u}\cdot\mathbf{i}+R^2\mathbf{u}\cdot\mathbf{u}}, \tag{7b}$$

$$\frac{\partial c}{\partial\tau}+\mathbf{u}\cdot\nabla c=\frac{\partial^2 c}{\partial x^2}+\varepsilon\left(\frac{\partial^2 c}{\partial y^2}+\frac{\partial^2 c}{\partial z^2}\right), \tag{8}$$

where the time derivative is the Lagrangian one. Here, the anisotropy parameter, $\varepsilon(=D_T/D_L)$, is the ratio of the transverse dispersion coefficient to the streamwise one. Here concentration, pressure, velocity and viscosity are nondimensionalized as $c=(C-C_+)/(C_--C_+)$, $p=K(P-P_-)/(\mu_- D_L)$, $\mathbf{u}=\mathbf{U}/(RU_0)$, $\mathbf{x}\{=(x, y, z)\}=RU_0(\mathbf{X}-\mathbf{i}U_0 t)/D_L$ and $\bar{\mu}=\mu/\mu_-$, respectively. For simplicity, from now on, we remove bars in the dimensionless space coordinates. In the present study, it is assumed that the viscosity is dependent on the concentration as

$$\bar{\mu}=\exp(-Rc), \tag{9}$$

where log-viscosity ratio $R\{=\ln(\mu_+/\mu_-)\}$ is constant. From the experimental findings, the fingering instabilities under the unidirectional flow in a porous medium have been assumed as two-dimensional flows, and therefore $\partial/\partial z$-terms have been usually ignored.

For the laminar region of $Re_K\leq 10^2$ [25], the basic concentration is represented in the following dimensionless form:

$$\frac{\partial c_0}{\partial\tau}=\frac{\partial^2 c_0}{\partial x^2}, \tag{10}$$

with the following initial and boundary conditions:

$$c_0(0, x)=1-H(x), \tag{11a}$$

$$c_0(\tau, x)\to 1 \text{ as } x\to-\infty \text{ and } c_0(\tau, x)\to 0 \text{ as } x\to\infty. \tag{11b}$$

Here H(x) is the Heaviside unit step function and x=0 is the interface position. By using the Laplace transform technique, the above concentration field can be solved as

$$c_0=\frac{1}{2}\operatorname{erfc}\left(\frac{\xi}{2}\right), \tag{12}$$

where $\xi=x/\sqrt{\tau}$.

THEORETICAL ANALYSIS

1. Linear Stability Equations

By linearizing the concentration field as $c(\tau, x, y)=c_0(\tau, x)+c_1(\tau, x, y)$, from Eqs. (5) and (6), the linear stability equations are derived as

$$\nabla p_1=-(\bar{\mu}_0+Re_K)\mathbf{u}-\left(\frac{1}{R}\frac{\partial\bar{\mu}}{\partial c}\Big|_{c_0}c_1+Re_K\mathbf{u}\cdot\mathbf{i}\right)\mathbf{i}, \tag{13}$$

$$\frac{\partial c_1}{\partial\tau}+u\frac{\partial c_0}{\partial x}=\frac{\partial^2 c_1}{\partial x^2}+\varepsilon\frac{\partial^2 c_1}{\partial y^2}, \tag{14}$$

where $c_0(\tau, x)$ and $c_1(\tau, x, y, z)$ are the base concentration and the concentration disturbance, respectively. In the above linear stability equations, we linearize ND and $\bar{\mu}$ as

$$ND=\sqrt{1+2R\mathbf{u}\cdot\mathbf{i}+R^2\mathbf{u}\cdot\mathbf{u}}\approx 1+R\mathbf{u}\cdot\mathbf{i}, \tag{15}$$

$$\bar{\mu}(c_0+c_1)\approx\bar{\mu}_0+\frac{\partial\bar{\mu}}{\partial c}\Big|_{c_0}c_1. \tag{16}$$

By taking double curls, we can obtain the following equation from Eq. (13):

$$\left(\frac{\partial^2}{\partial x^2}+\frac{\bar{\mu}_0+2Re_K}{\bar{\mu}_0+Re_K}\frac{\partial^2}{\partial y^2}\right)u-\frac{R\bar{\mu}_0}{\bar{\mu}_0+Re_K}\frac{\partial c_0}{\partial x}\frac{\partial u}{\partial x}=\frac{\bar{\mu}_0}{\bar{\mu}_0+Re_K}\frac{\partial^2 c_1}{\partial y^2}, \tag{17}$$

with the following boundary conditions:

$$c_1\to 0 \text{ and } u_1\to 0 \text{ as } x\to\pm\infty. \tag{18}$$

Through Fourier mode analysis, the above stability Eqs. (14) and (17) are reduced as

$$\frac{\partial c_1}{\partial\tau}+u\frac{\partial c_0}{\partial x}=\left(\frac{\partial^2}{\partial x^2}-\varepsilon k^2\right)c_1, \tag{19}$$

$$\left(\frac{\partial^2}{\partial x^2}-\frac{\bar{\mu}_0+2Re_K}{\bar{\mu}_0+Re_K}k^2\right)u-\frac{R\bar{\mu}_0}{\bar{\mu}_0+Re_K}\frac{\partial c_0}{\partial x}\frac{\partial u}{\partial x}=-\frac{\bar{\mu}_0}{\bar{\mu}_0+Re_K}k^2 c_1, \tag{20}$$

where k is a wavenumber showing spanwise periodicity. The above equations degenerate into those for Darcy's model discussed by Tan and Homsy [8] when $Re_K\to 0$.

In the present study, since the base concentration field is self-similar, by using the similarity variable ξ, the above stability equations can be rewritten in (τ, ξ)-domain as

$$\tau\frac{\partial c_1}{\partial\tau}=\left(\frac{\partial^2}{\partial\xi^2}+\frac{\xi}{2}\frac{\partial}{\partial\xi}-\varepsilon k^2\tau\right)c_1+\frac{\sqrt{\tau}}{2\sqrt{\pi}}\exp\left(-\frac{\xi^2}{4}\right)u, \tag{21}$$

$$\left\{\frac{\partial^2}{\partial\xi^2}+\frac{R\bar{\mu}_0}{\bar{\mu}_0+Re_K}\frac{1}{2\sqrt{\pi}}\exp\left(-\frac{\xi^2}{4}\right)\frac{\partial}{\partial\xi}-\frac{\bar{\mu}_0+2Re_K}{\bar{\mu}_0+Re_K}k^2\tau\right\}u=-k^2\tau\frac{\bar{\mu}_0}{\bar{\mu}_0+Re_K}c_1, \tag{22}$$

under the following conditions:

$$c_1\to 0 \text{ and } u\to 0 \text{ as } \xi\to\pm\infty. \tag{23}$$

It should be kept in mind that two sets of stability equations, Eqs. (18)-(20), and Eqs. (21)-(23), are mathematically equivalent. Therefore, from now on, we will conduct linear stability analysis by using Eqs. (21)-(23) as governing equations.

For the limiting case of $Re_K\to 0$ and $R\to 0$, Ryoo and Kim [26] solved the above stability equations analytically and numerically. Below, for some limiting case but not $Re_K\to 0$, we will solve the above stability equation analytically.

2. Initial Growth Rate

Let's try to find the growth rate of the disturbance for the limiting case of $\tau\to 0$. Regardless of the value of R, the above stability equations are reduced as

$$\tau\frac{\partial c_1}{\partial\tau}=\left(\frac{\partial^2}{\partial\xi^2}+\frac{\xi}{2}\frac{\partial}{\partial\xi}\right)c_1+\frac{\sqrt{\tau}}{2\sqrt{\pi}}\exp\left(-\frac{\xi^2}{4}\right)u, \tag{24}$$

$$\left\{\frac{\partial^2}{\partial\xi^2}+R\frac{\bar{\mu}_0+2Re_K}{\bar{\mu}_0+Re_K}\frac{1}{2\sqrt{\pi}}\exp\left(-\frac{\xi^2}{4}\right)\frac{\partial}{\partial\xi}\right\}u=0, \tag{25}$$

for the finite wavenumber disturbances. And the solution of the

velocity disturbance can be expressed as

$$u_1 = d_1 \int_{-\infty}^{\xi} \int_{1}^{exp(R)} \frac{\bar{\mu}_0 + 2Re_K}{\bar{\mu}_0 + Re_K} d\bar{\mu} d\xi' + d_2, \tag{26}$$

where the constants d_1 and d_2 should be zero to meet the boundary conditions: $u(\tau, \xi) \to 0$ as $\xi \to \pm\infty$. Therefore, regardless of the viscosity functional and Re_K-value, the final solution is $u \to 0$ as $\tau \to 0$. This means that initially there is no velocity disturbance and the instability motion is driven by the concentration disturbance.

Then, the concentration disturbance is governed by

$$\tau \frac{\partial c_1}{\partial \tau} = \left(\frac{\partial^2}{\partial \xi^2} + \frac{\xi}{2} \frac{\partial}{\partial \xi} \right) c_1. \tag{27}$$

By expressing the concentration disturbance as

$$c_1(\tau, \xi) = \sum_{i=0}^{\infty} a_i(\tau) \kappa_i H_i\left(\frac{\xi}{2}\right) \exp\left(-\frac{\xi^2}{4}\right), \tag{28}$$

Kim [25] shows analytically that the least stable disturbance and its growth rate are

$$c_1(\tau, \xi) = a_0(\tau) \kappa_0 \exp\left(-\frac{\xi^2}{4}\right), \tag{29a}$$

$$\sigma^* \left(= \frac{1}{a_0} \frac{da_0}{d\tau} \right) = -\frac{1}{2\tau}, \tag{29b}$$

where H_i is the i-th Hermite polynomial and κ_i is its weighting factor. The above findings mean that initially the system is unconditionally stable since the least stable disturbance has a negative growth rate. The present initial growth rate analysis is totally different from that based on the conventional QSSA, which gives positive initial growth rate. This discrepancy will be discussed later. It is stressed that no assumption is introduced and therefore the present analysis gives an exact solution. Also, this analysis can be applied to the long-wave limit $k \to 0$ and finite time, *i.e.*, $k\sqrt{\tau} \to 0$.

3. For the limiting case of $R \to 0$

Because the viscosity functional becomes $\bar{\mu}_0 \to 1$ as $R \to 0$, the governing Eq. (22) can be degenerated as

$$\left(\frac{\partial^2}{\partial \xi^2} - \frac{1 + 2Re_K}{1 + Re_K} k^2 \tau \right) u = -\frac{1}{1 + 2Re_K} \frac{1 + 2Re_K}{1 + Re_K} k^2 \tau c_1, \tag{30}$$

By combining Eqs. (28) and (30), we can obtain the following velocity disturbance:

$$u_1(\tau, \xi) = \frac{1}{1 + 2Re_K} \sum_{i=0}^{\infty} a_i(\tau) \kappa_i \phi_i(\xi), \tag{31}$$

where $\phi_i(\xi)$ is the solution of the following ordinary differential equation:

$$(D^2 - l^{*2}) \phi_i = -l^{*2} H_i\left(\frac{\xi}{2}\right) \exp\left(-\frac{\xi^2}{4}\right), \tag{32}$$

Under the following boundary conditions:

$$\phi_i \to 0 \text{ as } \xi \to \pm\infty, \tag{33}$$

where $D = d/d\xi$, $l^* = \left(\frac{1 + 2Re_K}{1 + Re_K}\right)^{1/2} k^*$ and $k^* = k\sqrt{\tau}$. The analytic and closed form solution of Eqs. (32) and (33) is given in Appendix.

By combining Eqs. (21), (28) and (31), we can get the following relation:

$$\frac{d\mathbf{A}}{d\tau} = \mathbf{E}\mathbf{A}, \tag{34a}$$

where

$$\mathbf{A} = [a_0, a_1, a_2, \cdots]^T, \tag{34b}$$

$$[\mathbf{E}]_{ij} = \int_{-\infty}^{\infty} \exp\left(\frac{\xi^2}{4}\right) \phi_j \left(\frac{\partial^2}{\partial \xi^2} + \frac{\xi}{2} \frac{\partial}{\partial \xi} - \varepsilon k^{*2} \right) \phi_i d\xi - \frac{1}{1 + 2Re_K} \frac{1}{2\sqrt{\pi}} R^* \int_{-\infty}^{\infty} \phi_j \psi_i d\xi = -(\lambda_i + \varepsilon k^{*2}) \delta_{ij} - \frac{1}{1 + 2Re_K} \frac{1}{2\sqrt{\pi}} R^* \int_{-\infty}^{\infty} \phi_j \psi_i d\xi \tag{34c}$$

The least stable disturbance given by Eq. (29) corresponds to

$$\mathbf{A} \to [a_0, 0, 0, \cdots]^T \text{ as } \tau \to 0, \tag{35}$$

which is the proper initial condition for Eq. (34).

4. Quasi-steady State Approximation (QSSA)

Except for the above limiting cases, we cannot solve Eq. (21) analytically; therefore, we should depend on QSSA and numerical solution. By employing QSSA in the similar (τ, ξ)-domain, *i.e.*, QSSAξ, the disturbance quantities can be approximated as [9,10,25]

$$[u(\tau, \xi), c_1(\tau, \xi)] = [\bar{u}(\xi), \bar{c}_1(\xi)] \exp(\sigma^* \tau). \tag{36}$$

By substituting the above approximation into Eqs. (21)-(23), we can get the following stability equations:

$$\left(D^2 + \frac{\xi}{2} D - \varepsilon k^{*2} - \sigma^* \tau \right) \bar{c}_1 = -\frac{\tau^{1/2}}{2\sqrt{\pi}} \exp\left(-\frac{\xi^2}{4}\right) \bar{u}, \tag{37}$$

$$\left\{ D^2 + \frac{R\bar{\mu}_0}{\bar{\mu}_0 + Re_K} \frac{1}{2\sqrt{\pi}} \exp\left(-\frac{\xi^2}{4}\right) D - \frac{\bar{\mu}_0 + 2Re_K}{\bar{\mu}_0 + Re_K} k^{*2} \right\} \bar{u} = -k^{*2} \frac{\bar{\mu}_0}{\bar{\mu}_0 + Re_K} \bar{c}_1, \tag{38}$$

$$\bar{c}_1 \to 0 \text{ and } \bar{u}_1 \to 0 \text{ as } \xi \to \pm\infty. \tag{39}$$

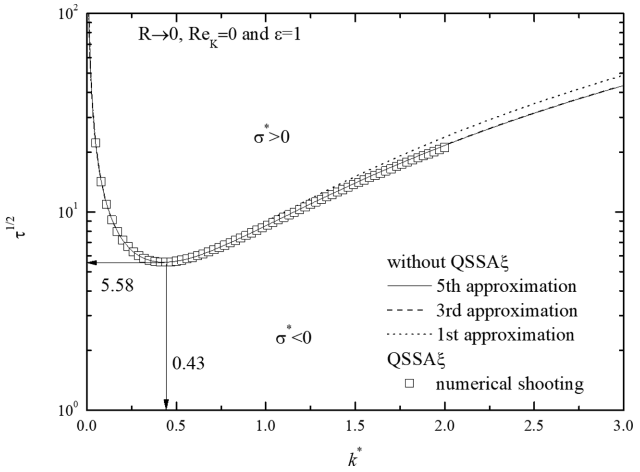

Fig. 2. Neutral stability curves for the limiting case of $R \to 0$, $Re_K = 0$ and $\varepsilon = 1$. Analytic approximations without QSSAξ are explained in the reference [26] and the Appendix.

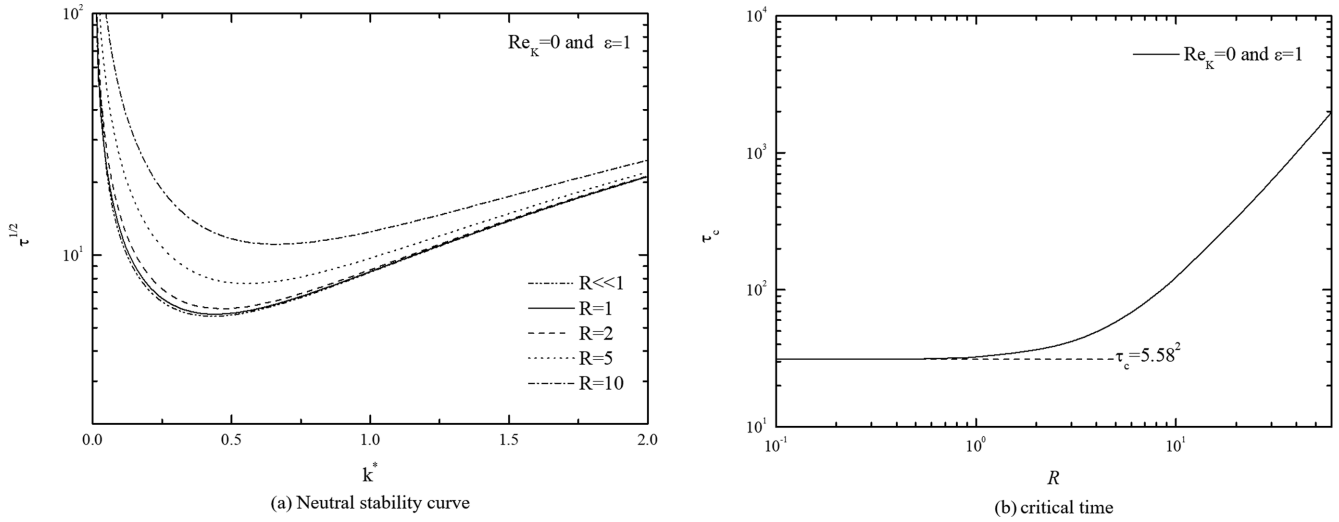

Fig. 3. Effect of viscosity contrast parameter R on the neutral stability curves for the case of Re_K=0 and ε=1. (a) Neutral stability curve and (b) critical time.

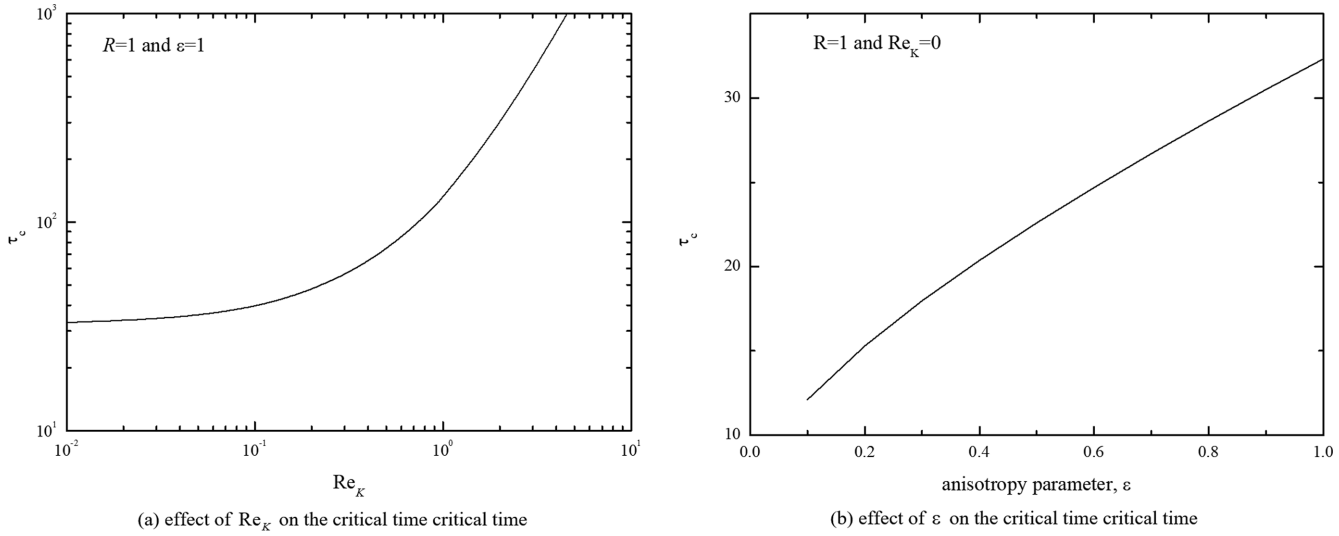

Fig. 4. Effect of (a) Re_K and (b) ε on the critical time for the case of R=1.

where D=d/dξ. This QSSA in the (τ, ξ)-domain has been widely used in the similar problems [26,27].

The above stability Eqs. (36)-(38) are solved using the outward shooting method [28,29]. For the limiting case of $Re_K \to 0$ and $R \to 0$, the comparison between the present numerical shooting solution with Ryoo and Kim's [26] analytic solution is given in Fig. 2. As shown in this figure, the present analytic and numerical solutions are in good agreement. For the base system of Re_K=0 and ε=1, the neutral stability curves of the various R cases are compared in Fig. 3. For the limiting case of $Re_K \to 0$ and $R \to 0$, the following stability limits with and without the quasi-steady state approximation (QSSA) were suggested:

$$\tau_c\left\{=X_c\frac{R^2U_0}{D_L}\right\}=5.58^2 \text{ and } \frac{2\pi}{\lambda_c}\left(\frac{D_L}{RU_0}\right)=\frac{0.43}{5.58}$$

for $Re_K \to 0$, $R \to 0$ and ε=1. (40a&b)

In addition, the effect of and on the linear stability is summarized in Fig. 4, which shows that both Re_K and ε make the system stable and, therefore, retard the onset of the VF instability.

NUMERICAL SIMULATIONS

1. Stream Function-vorticity Formulation

Viscous fingering phenomena have been solved numerically by using various numerical methods, such as the pseudo-spectral method [11,12], the finite element method [16], and the lattice Boltzmann method [30]. Using the stream function $\psi(\tau, x, y)$, such that $\mathbf{u}=(\partial\psi/\partial y, -\partial\psi/\partial x, 0)$, and the relation of $c(\tau, x, y)=c_0(\tau, x)+c_1(\tau, x, y)$, the governing Eqs. (4)-(7) can be rewritten as

$$\nabla^2\psi=-\omega_z, \tag{41}$$

$$\omega_z=\frac{\bar{\mu}}{\bar{\mu}+\mathrm{Re}_K\mathrm{ND}}\left\{-\frac{\partial c_1}{\partial y}\left(1+R\frac{\partial\psi}{\partial y}\right)-R\left(\frac{\partial c_0}{\partial x}+\frac{\partial c_1}{\partial x}\right)\frac{\partial\psi}{\partial x}\right\} \tag{42a}$$

$$+\frac{\mathrm{Re}_K}{\bar{\mu}+\mathrm{Re}_K\mathrm{ND}}\frac{1}{\mathrm{ND}}\left[\begin{array}{l}\left\{\left(\frac{\partial^2\psi}{\partial y^2}\right)+R\left(\frac{\partial\psi}{\partial y}\right)\left(\frac{\partial^2\psi}{\partial y^2}\right)+R\left(\frac{\partial\psi}{\partial x}\right)\left(\frac{\partial^2\psi}{\partial x\partial y}\right)\right\}\left(1+R\frac{\partial\psi}{\partial y}\right)\\ +R\left\{\left(\frac{\partial^2\psi}{\partial x\partial y}\right)+R\left(\frac{\partial\psi}{\partial y}\right)\left(\frac{\partial^2\psi}{\partial x\partial y}\right)+R\left(\frac{\partial\psi}{\partial x}\right)\left(\frac{\partial^2\psi}{\partial x^2}\right)\right\}\frac{\partial\psi}{\partial x}\end{array}\right],$$

$$\mathrm{ND}=\sqrt{1+2R\left(\frac{\partial\psi}{\partial y}\right)+R^2\left(\frac{\partial\psi}{\partial y}\right)^2+R^2\left(\frac{\partial\psi}{\partial x}\right)^2}, \tag{42b}$$

$$\frac{\partial c_1}{\partial\tau}+\frac{\partial\psi}{\partial y}\left(\frac{\partial c_0}{\partial x}+\frac{\partial c_1}{\partial x}\right)-\frac{\partial\psi}{\partial x}\frac{\partial c_1}{\partial y}=\left(\frac{\partial^2 c_1}{\partial x^2}+\varepsilon\frac{\partial^2 c_1}{\partial y^2}\right), \tag{43}$$

For Darcy's limit, Eq. (42) is reduced as

$$\omega_z=-R\left(\frac{\partial c_0}{\partial x}+\frac{\partial c_1}{\partial x}\right)\frac{\partial\psi}{\partial x}-\frac{\partial c_1}{\partial y}\left(1+R\frac{\partial\psi}{\partial y}\right). \tag{44}$$

The proper boundary conditions are

$$c_1\to 0 \text{ and } \psi\to 0 \text{ as } x\to\pm\infty. \tag{45}$$

Along the transverse boundaries, we imposed periodic conditions.

2. Linear Analysis

Prior to conducting full nonlinear analysis, it is helpful to test the solution method for the linear region where the previous linear analysis can apply. For a linear region, by neglecting the nonlinear terms, we can simplify Eqs. (42) and (43) as

$$\omega_z=\frac{\bar{\mu}}{\bar{\mu}+\mathrm{Re}_K\mathrm{ND}}\left\{-\frac{\partial c_1}{\partial y}-R\left(\frac{\partial c_0}{\partial x}\right)\frac{\partial\psi}{\partial x}\right\}+\frac{\mathrm{Re}_K}{\bar{\mu}+\mathrm{Re}_K\mathrm{ND}}\frac{1}{\mathrm{ND}}\left(\frac{\partial^2\psi}{\partial y^2}\right), \tag{46a}$$

$$\mathrm{ND}=1+R\left(\frac{\partial\psi}{\partial y}\right), \tag{46b}$$

$$\frac{\partial c_1}{\partial\tau}+\frac{\partial\psi}{\partial y}\frac{\partial c_0}{\partial x}=\left(\frac{\partial^2 c_1}{\partial x^2}+\varepsilon\frac{\partial^2 c_1}{\partial y^2}\right), \tag{47}$$

under the boundary conditions (44). To solve the linearized governing equations, *i.e.*, Eqs. (39), (44) and (45), we introduced the following initial condition at initiation time τ_i:

$$c_1(\tau_i, x)=a_0(\tau_i)\frac{1}{\sqrt{2\sqrt{\pi}}}\exp\left(-\frac{x^2}{4\sqrt{\tau_i}}\right)\cos(ky), \tag{48}$$

which corresponds to Eqs. (29) and (35). In the present study, the above linearized Eqs. (44) and (45) are solved by using Fourier spectral method, which has been widely used in the similar problems [26,31]. The calculation domain is set to $(l_x, l_y)=(500, \lambda)$, where $\lambda(=2\pi/k)$ is the wavelength corresponding to the wavenumber k. The growth rate of disturbance is determined as [8,18]

$$\sigma(\tau)=\frac{1}{\Delta\tau}\ln\left(\frac{\|c_1\|_{\tau+\Delta\tau}}{\|c_1\|_\tau}\right), \tag{49a}$$

where

$$\|c_1\|_\tau=\left[\int_{-l_y/2}^{l_y/2}\int_0^{l_x}c_1^2(\tau, x, y)\,dy\,dx\right]^{1/2}. \tag{49b}$$

The present linear analysis corresponds to the initial value calculation of (IVC) Tan and Homsy [8] and Yuan and Azaiez [18].

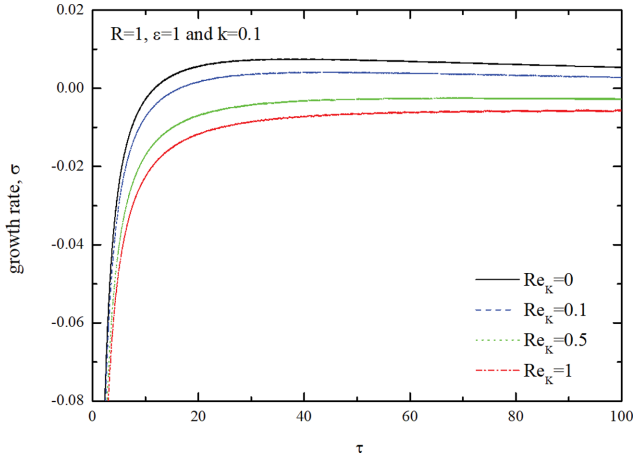

Fig. 5. Effect of Re_K on the growth rate of disturbance for the case of R=1, ε=1 and k=0.1.

For the exemplary case of R=1 and ε=1, the effect of non-linear drag on the growth rate are summarized in Fig. 5. As shown in this figure, the disturbance has large negative growth rate regardless of Re_K. Similar trend can be shown in the IVC of Tan and Homsy [8] and Yuan and Azaiez [18], even though they introduced random initial condition rather than the present one, Eq. (45). Tan and Homsy [8], Yuan and Azaiez [18] and the present findings say that the system is initially stable for the small amplitude disturbances. These numerical IVC results are consistent with the present initial growth rate analysis given in the section 3.2. Furthermore, from the present study, it can be said that the non-linear drag make the system stable, *i.e.*, suppresses the growth of the disturbances.

3. Nonlinear Simulations

In the previous linear analysis, we only considered a single mode disturbance, i.e., the wavelength of the disturbances is fixed throughout the simulation. However, nonlinear phenomena, such as the wavelength selection and the enhancement of mass transfer rate and mixing, cannot be observed in the single-mode linear analysis. In this section, the simulation domain is set to $[-10^3, 10^3]\times[-10^3, 10^3]$, and 2,048×2,048 collocation points are used. Since the linear stability analysis cannot suggest the dominant initial wavenumber, in the present simulation the following initial condition is employed:

$$c_1(\tau_i, x)=a_0(\tau)\frac{1}{\sqrt{2\sqrt{\pi}}}\exp\left(-\frac{x^2}{4\sqrt{\tau_i}}\right)\mathrm{rand}(y), \tag{50}$$

where $a_0(\tau_i)$ means the disturbance level at $\tau=\tau_i$, and rand(y), which is the pseudo-random number uniformly distributed between −1 and 1, is introduced not to fix the single mode disturbance. In the present study, we set $a_0(\tau_i)=0.01$ and $\tau_i=0.1$. The effect of the initiation condition on the nonlinear phenomena is summarized in the previous studies [31,32].

The variation of mixing length has been used to quantify the nonlinear effects [15]. However, in the present study, let us consider the mass transfer rate to characterize the fingering motion. The dimensionless total mass flux at the initial displacing position x=0, J, can be obtained as the sum of the diffusional flux, J_0 and

the convective one, J_1:

$$J = J_0 + J_1. \tag{51}$$

The diffusional flux can be computed explicitly from the base concentration profile, Eq. (10), as

$$J_0 = -\left.\frac{\partial c_0}{\partial x}\right|_{x=0} = \frac{1}{2\sqrt{\pi\tau}}. \tag{52}$$

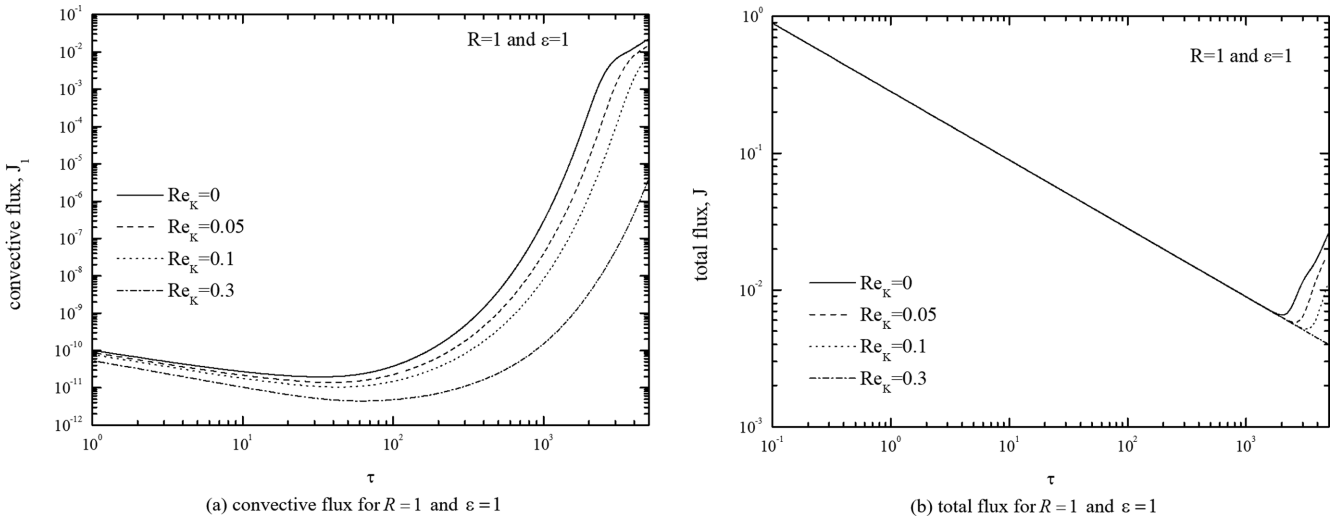

Fig. 6. Effect of Re_K on the temporal evolutions of convective and total fluxes. (a) Convective flux for R=1 and ε=1, (b) total flux for R=1 and ε=1.

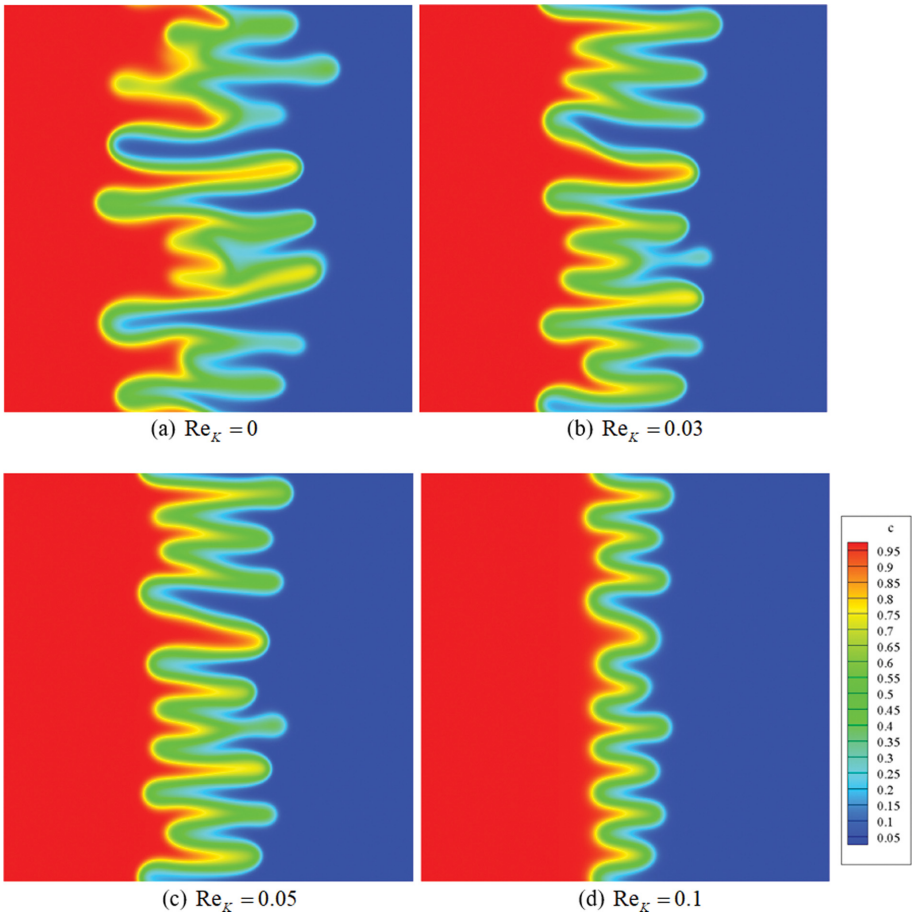

Fig. 7. Effect of Re_K-value on the concentration fields for R=1 and τ=5×10^3. (a) Re_K=0, (b) Re_K=0.03, (c) Re_K=0.05 and (d) Re_K=0.1. Plotting domain is [−10^3, 10^3]×[0, 2×10^3].

The fluxes from fingering motion are obtained as [33]

$$J_1=\frac{1}{l_y}\int_0^{l_y}\left\{-\left.\frac{\partial c_1}{\partial x}\right|_{x=0}\right\}dy=\frac{1}{l_x l_y}\int_{-l_x/2}^{l_x/2}\int_0^{l_y}uc_1\,dy\,dx. \tag{53}$$

The effects of the non-linear drag and the viscosity contrast on the mass transfer rates and the concentration fields are summarized in Figs. 6 and 7, which show that the inertia effects which are characterized by Re_K making the system stable and, therefore, retarding the onset and the growth of instability. For the buoyancy-driven instability problem, based on the systematic experiments and linear stability analysis, Chung et al. [20] concluded that the inertia and dispersion effects are predominant for $Re_K>0.1$. From the present linear and nonlinear analyses summarized in Figs. 5-7, it is clear that the onset of instability and the development of instability motions are strongly influenced by Re_K.

RESULTS AND DISCUSSION

Most of the previous studies have solved Eqs. (4)-(6) by introducing the quasi-steady state approximation in (τ, x)-domain (QSSAx) or frozen-time model [8,17]. Under the QSSAx, the disturbance quantities are expressed as

$$[u_1(\tau, x), c_1(\tau, x)]=[\bar{u}_1(x), \bar{c}_1(x)]\exp\{\sigma\tau\}. \tag{54}$$

For the extreme case of $\tau=0$, by expressing the base concentration file as

$$c_0(0, x)=1-H(x) \text{ and } \frac{\partial c_0}{\partial x}=-\delta(x), \tag{55}$$

where H(x) and δ(x) are the Heaviside step function and Dirac delta function, respectively, we can get the following dispersion relation and corresponding disturbance fields:

$$2s(p_-+e^R p_+)(s+p_-)(s+p_+)-e^R q_+^2(s+p_-)-q_-^2(s+p_+)=0, \tag{56}$$

where

$$s=(\varepsilon k^2+\sigma)^{1/2},\ p_-^2=\frac{(1+2Re_K)}{(1+Re_K)}k^2,\ p_+^2=\frac{(e^R+2Re_K)}{(e^R+Re_K)}k^2,$$
$$q_-^2=\frac{Rk^2}{(1+Re_K)} \text{ and } q_+^2=\frac{e^R Rk^2}{(e^R+Re_K)}. \tag{57}$$

For the limiting case of $Re_K=0$ and $\varepsilon=1$, Eq. (57) is reduced as

$$\sigma=\frac{k}{2}(R-k-\sqrt{k^2+2kR}) \text{ for } \tau=0,\ Re_K=0 \text{ and } \varepsilon=1, \tag{58}$$

which is identical with Tan and Homsy's [8] initial growth rate. The non-linear drag effect on the initial grow rate based on the convectional QSSAx is featured in Fig. 8. Also, based on the present QSSAξ, the non-linear drag effect on the critical time is summarized in Fig. 9. As shown Figs. 8 and 9, the non-linear drag term stabilizes the present system. Furthermore, the conventional QSSAx suggests that the system is unstable whenever R>0. However, Tan and Homsy and the present IVC results show large negative growth rates for the case of $\tau<<1$ (see Figs. 7-10 of Tan and Homsy [8]). Due to this discrepancy, as discussed by Tan and Homsy [8], special care should be taken for the growth rate from the conventional QSSAx.

As shown in Eq. (26b), unlike the initial growth rate analysis based on the QSSAx, the present analysis yields that the system is initially stable. Also, the present IVC gives a similar trend (see Fig. 5). Therefore, the discrepancy between the QSSAx and IVC is resolved through the present initial growth rate analysis. Furthermore, the present initial growth rate study explains experimental findings. Slobod and Thomas [4] experimentally showed that near the initial displacing front, no fingering is found in the low flow rate experiment (see Fig. 1 of Slobod and Thomas [4]) and a single bulging finger is observed at the far downstream (see Fig. 1 of Slobod and Thomas [4]). Later Perkins et al. [34] reported, in their Table 1, the experimentally determined critical length from which the fingering motion was observed. From these experimental results, there may exist a critical length, or critical time, to develop a fingering instability even for the case of unfavorable viscosity distribution. These experimental findings cannot be explained by the

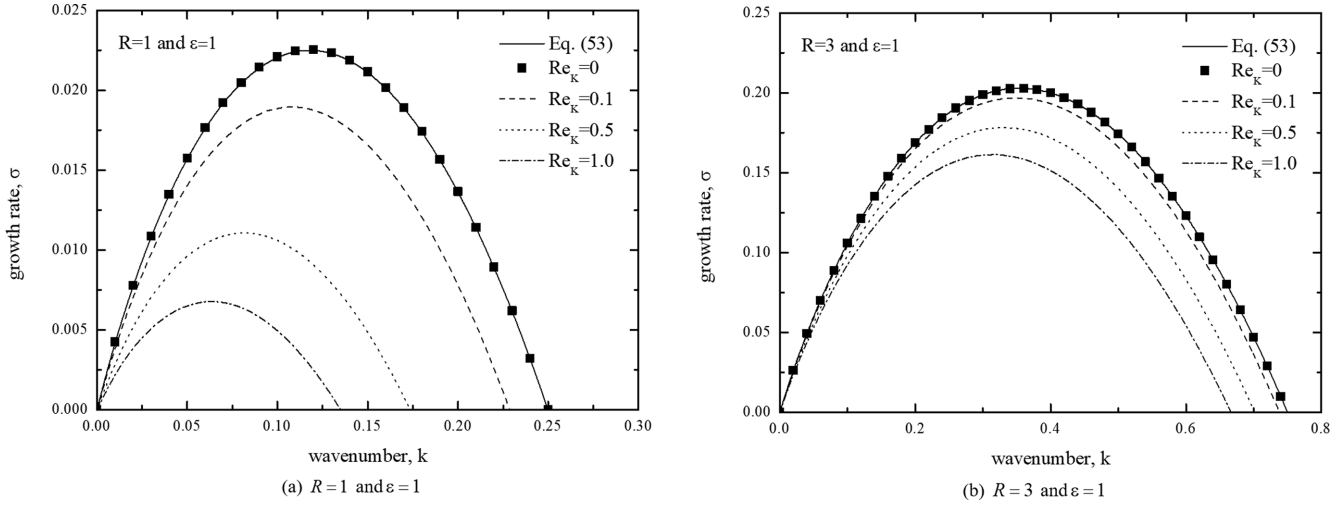

Fig. 8. Effect of Re_K on the initial growth rate obtained from the QSSAx. (a) R=1 and ε=1, (b) R=3 and ε=1.

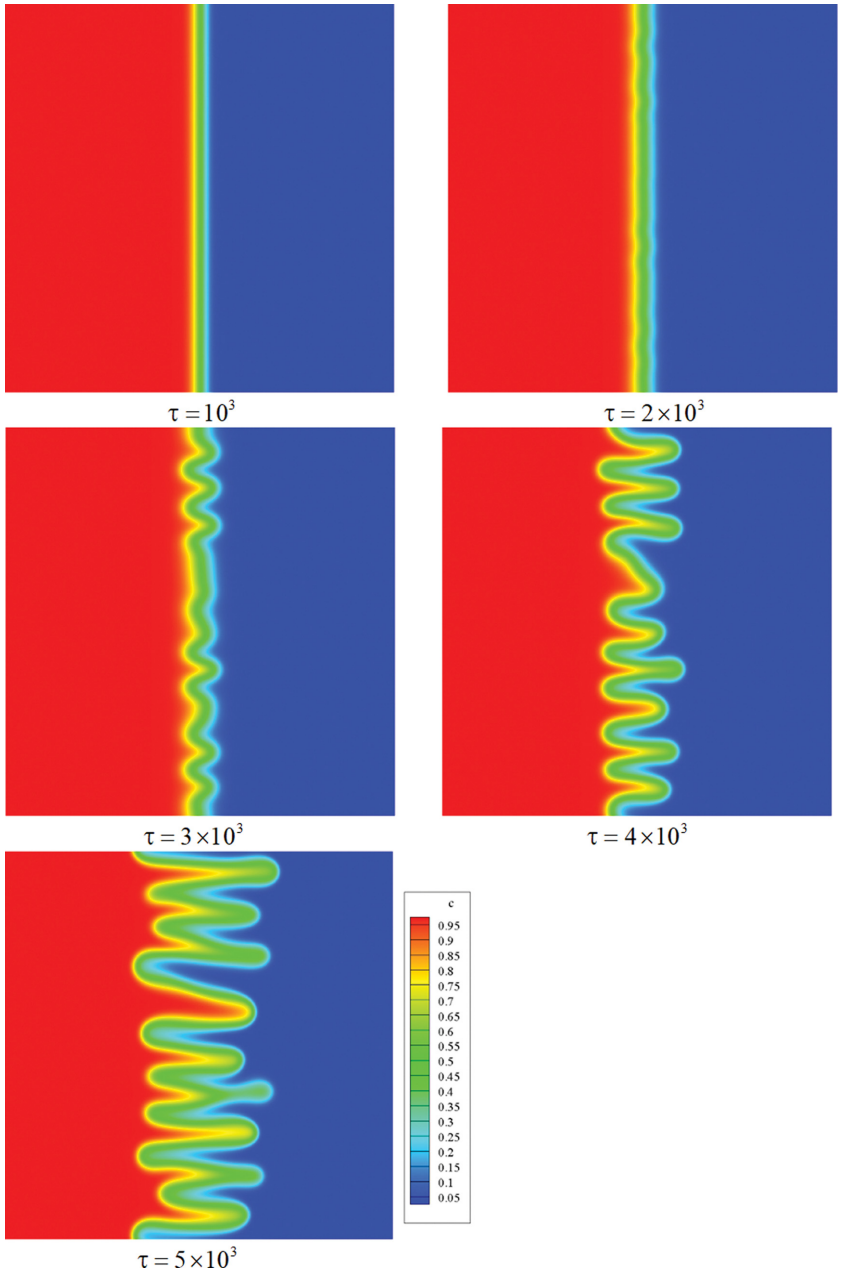

Fig. 9. Temporal evolution of the concentration field for the case of R=1 and Re_K=0.05. Plotting domain is $[-10^3, 10^3]\times[-10^3, 10^3]$.

conventional QSSAx, which yields maximum growth rate at τ=0. However, as shown in Figs. 2-4, the present QSSAξ can produce the critical time from which the system is unstable and the corresponding critical wavenumber.

The critical time summarized in Figs. 3 and 4 corresponds to the time at which the infinitesimal disturbance starts to grow. However, it is well-known that the growth period of instability is required to grow the infinitesimal disturbance to the experimentally observable motion. So, fully non-linear numerical simulations are needed to predict experimental data qualitatively, even though the present linear analysis can explain the experimental results qualitatively. In the present study, fully non-linear simulations were also conducted by using high accuracy Fourier-spectral method. As shown in Fig. 6, there exist two characteristic times: one is the critical time, τ_c, at which the disturbance flux starts to grow, and the other is the minimum time, τ_m, at which the total flux reaches its minimum. The former can be thought of as the critical time from which the disturbances start to grow, and the latter is regarded as the time from which the non-linear effects can be detectible. For an example case of R=1 and ε=1, the effect of the non-linear drag on the onset and the growth of disturbance is summarized in Figs. 6 and 7. This figure shows that the non-linear drag plays an important role in the linear and non-linear growth of instability.

For the specific case of R=1, ε=1 and Re_K=0.05, the evolution of the concentration disturbance is explained in Fig. 9. This figure shows that nonlinear competition yields a series of cells of slightly

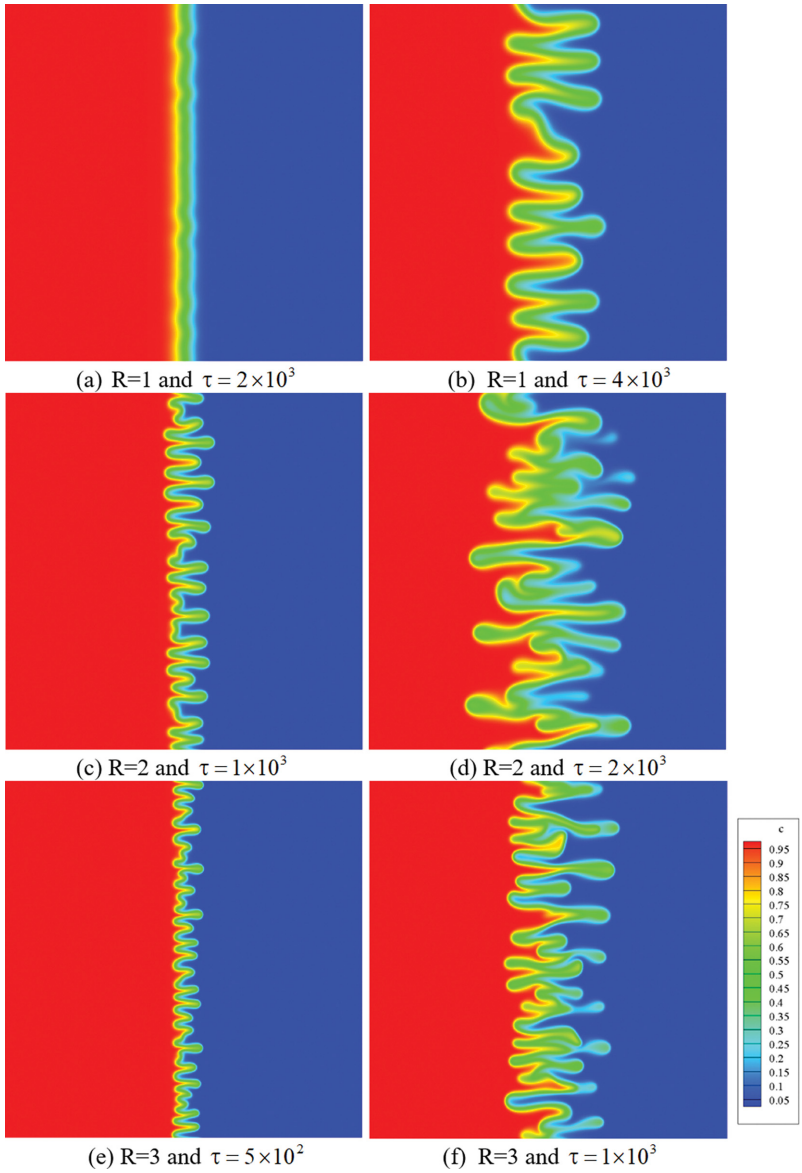

Fig. 10. Effect of R-value on the concentration fields for Re_K=0.03. Plotting domain is $[-10^3, 10^3]\times[-10^3, 10^3]$.

different widths and amplitudes. As these cells grow, less viscous cells advance and more viscous ones retreat and thus such cells will eventually advect away from the region close to the original interface. This provides a natural secondary instability mechanism which could include cell-merging and therefore an increase in the wavelength. The effect of the nonlinear drag on the evolution of the concentration field is featured in Fig. 10. As discussed previously, the non-linear drag suppresses the growth of instability motion.

Now, we focused on the effect of R on the growth of the instability motion. For the case of Re_K=0, the effect of R on the temporal evolution of the total flux and the snapshot of the concentration field are summarized in Figs. 11 and 12. Form this figure, it can be concluded that for the limiting case of Re_K=0, the terms associated with R make the system stable in the present rescaled time and space domain, *i.e.*, suppress the onset of instability and retard the growth of instability However, its stabilization effects are not

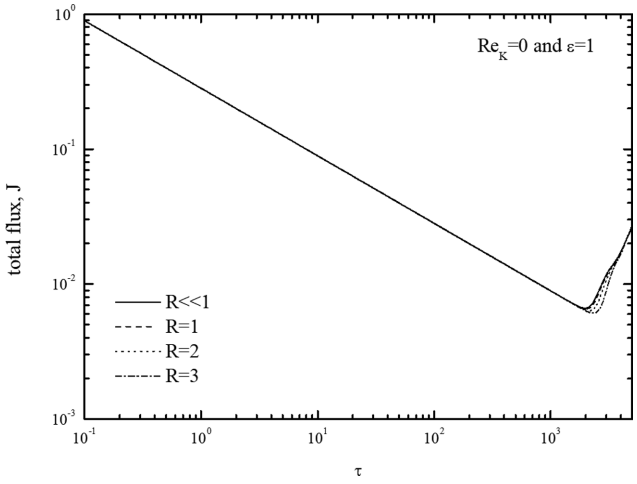

Fig. 11. Effect of R-value on the temporal evolution of the total flux.

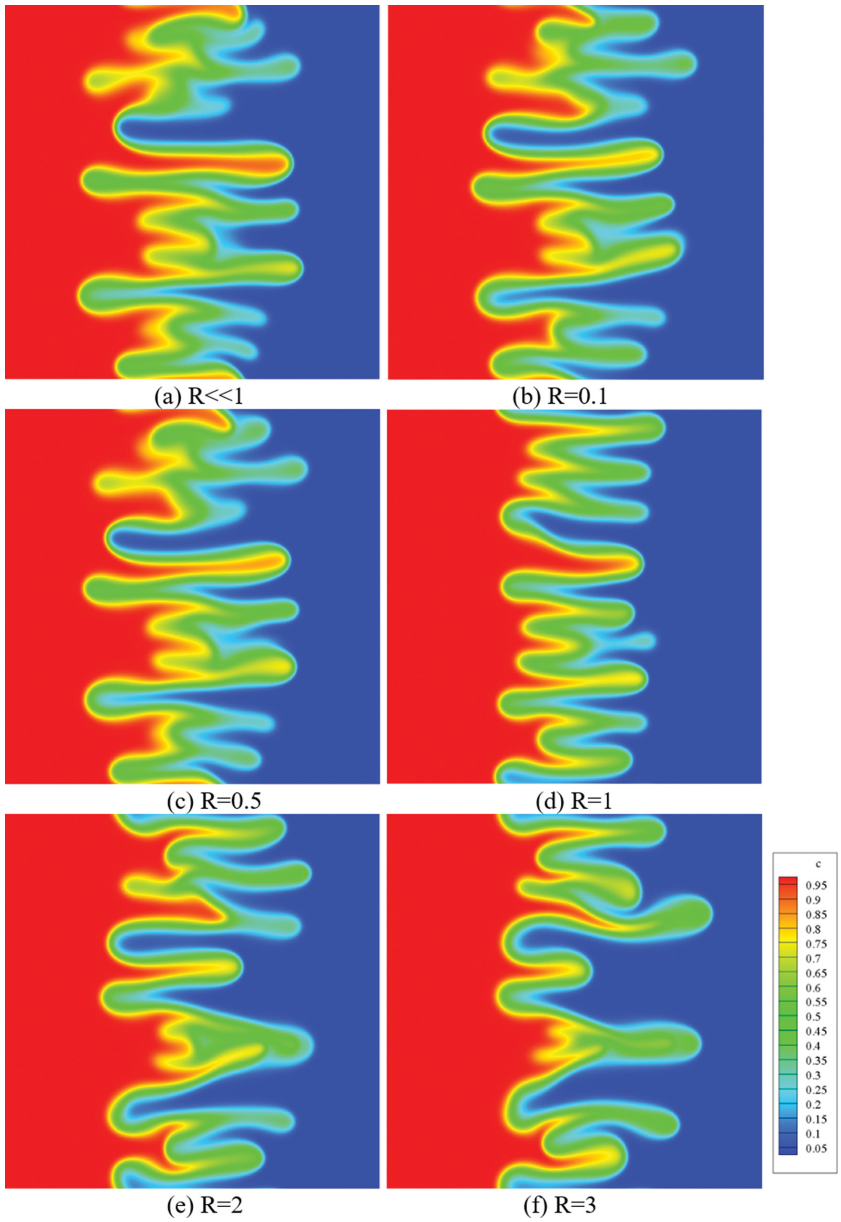

Fig. 12. Effect of R-value on the concentration fields for Re_K=0 and τ=5×10^3. (a) R<<1, (b) R=0.1, (c) R=0.5, (d) R=1, (e) R=2 and (f) R=3. Plotting domain is [−10^3, 10^3]×[−10^3, 10^3].

significant for R≤3.

For the case of Re_K=0.03, the results of the nonlinear simulations are summarized in Figs. 13 and 14. These figures imply that the effect of the nonlinear drag on the growth of instability is remarkable for R<1. To explain this fact, we take the limit on the relation (57) as R→0:

$$\omega_z \to \frac{1}{1+\mathrm{Re}_K}\left\{-\frac{\partial c_1}{\partial y}+\mathrm{Re}_K\left(\frac{\partial^2 \psi}{\partial y^2}\right)\right\} \text{ as } R\to 0. \tag{59}$$

The above limit suggests that for the small R-system, the stabilizing effects of nonlinear drag, $\partial^2\psi/\partial y^2$, overwhelm the driving force of the instability, $-\partial c/\partial y$. Thus, the nonlinear drag effects should be considered even for the small R system. In addition, the effect of the anisotropic parameter, ε, on the VF instability field is summarized in Fig. 15. As discussed in the above linear stability section, ε makes the system stable, *i.e.*, suppresses the development of VF motion.

CONCLUSIONS

The non-linear drag effect on the onset and growth of viscous fingering was analyzed theoretically and numerically. Employing Forchheimer's extension as the momentum equation to explain the flow in a porous medium, new stability equations were derived under linear stability theory and solved analytically and numerically with and without a quasi-steady state approximation. Through the initial growth rate analysis, we showed that initially the present system is unconditionally stable and suggest the most unstable distur-

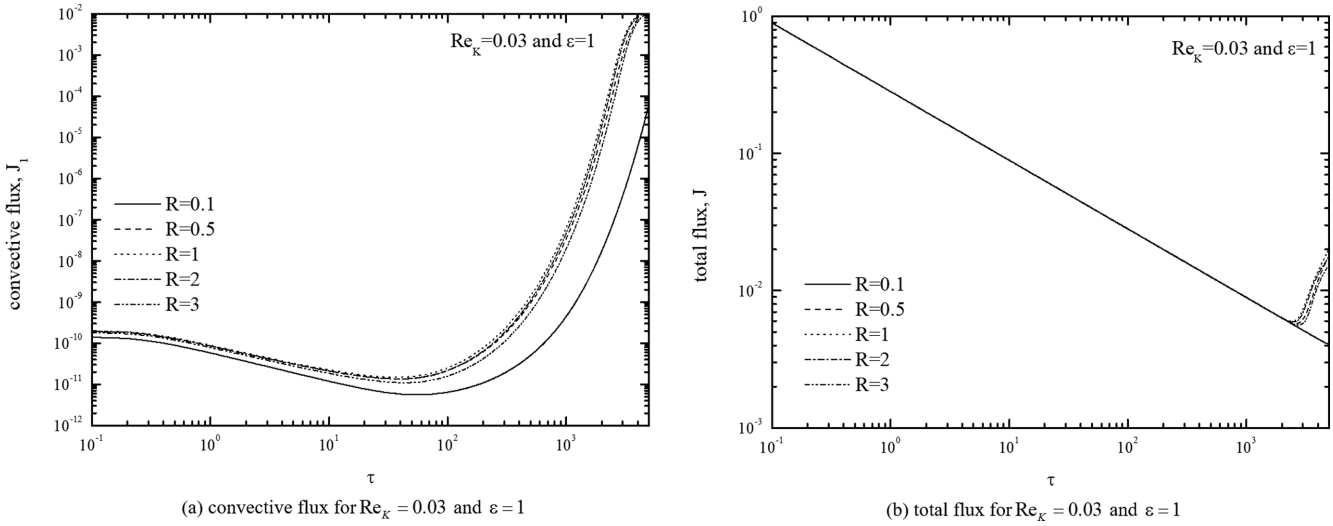

Fig. 13. Effect of the viscosity contrast parameter R on the temporal evolutions of convective and total fluxes. (a) Convective flux for Re_K= 0.03 and ε=1 and (b) total flux for Re_K=0.03 and ε=1.

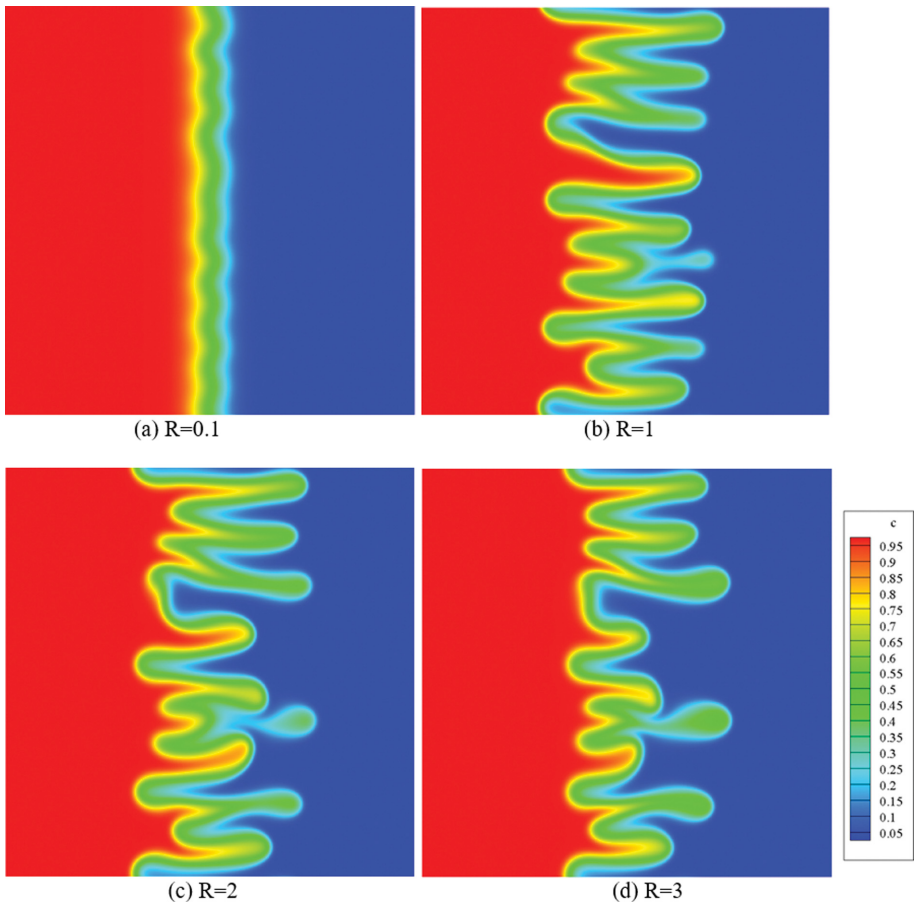

Fig. 14. Effect of R-value on the concentration fields for Re_K=0.03 and τ=5×10^3. (a) R=0.1, (b) R=1, (c) R=2 and (d) R=3. Plotting domain is [−10^3, 10^3]×[−10^3, 10^3].

bance as a deterministic form. Using the linear stability results as an initial condition, fully non-linear numerical simulations were conducted using the Fourier spectral method. The present theoretical and numerical analyses yield that the non-linear drag impedes the onset and growth of instability motion. Furthermore, the present non-linear simulations propose that the wavelength of the fingering motion increases as the time goes on. All of the present findings are consistent with the previous experimental ones.

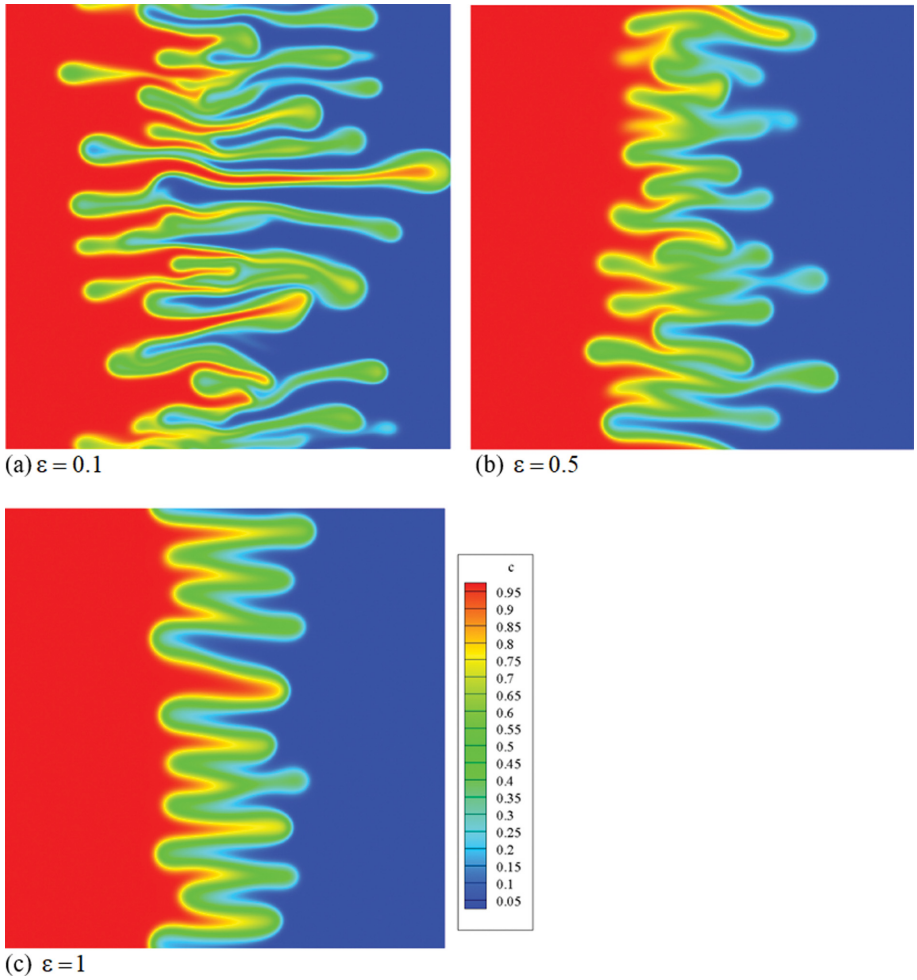

Fig. 15. Effect of ε-value on the concentration fields for Re_K=0.03, R=1, and τ=5×10^3. (a) ε=0.1, (b) ε=0.5, and (c) ε=1. Plotting domain is [−10^3, 10^3]×[−10^3, 10^3].

ACKNOWLEDGEMENT

This research was supported by the 2021 scientific promotion program funded by Jeju National University.

REFERENCES

1. S. Hill, *Chem. Eng. Sci.*, **1**, 247 (1952).
2. G. M. Homsy, *Ann. Rev. Fluid Mech.*, **19**, 271 (1987).
3. S. G. Subraveti, P. Nikrityuk and A. Rajendran, *J. Chromatogr. A*, **1534**, 150 (2018).
4. R. L. Slobdo and R. A. Thomas, *Soc. Pet. Eng. J.*, **3**, 9 (1963).
5. L. D. Plante, P. M. Romano and E. J. Fernandez, *Chem. Eng. Sci.*, **49**, 2229 (1994).
6. B. S. Broyles, R. A. Shalliker, D. E Cherrak and G. Guiochon, *J. Chreomatogr. A*, **822**, 173 (1998).
7. M. L. Dickson, T. T. Norton and E. J. Fernandez, *AIChE J.*, **43**, 409 (1997).
8. C. T. Tan and G. M. Homsy, *Phys. Fluids*, **29**, 3549 (1986).
9. S. Pramanik and M. Mishra, *Phys. Fluids*, **25**, 074104 (2013).
10. S. Pramanik and M. Mishra, *Chem. Eng. Sci.*, **110**, 144 (2014).
11. S. Pramanik and M. Mishra, *Chem. Eng. Sci.*, **122**, 523 (2015).
12. S. Pramanik and M. Mishra, *Europhys. Lett.*, **109**, 64001 (2015).
13. T. K. Hota and M. Mishra, *J. Fluid Mech.*, **856**, 552 (2018).
14. M. C. Kim and C. K. Choi, *J. Non-Newtonian Fluid Mech.*, **166**, 1211 (2011).
15. M. R. Shoghi and M. Norouzi, *Rheol Acta*, **54**, 973 (2015).
16. M. Norouzi, S. Dorrania, H. Shokria and O. A. Bég, *Int. J. Heat Mass Transfer*, **129**, 212 (2019).
17. Q. Yuan and J. Azaiez, *Can. J. Chem. Eng.*, **93**, 1490 (2015).
18. Q. Yuan and J. Azaiez, *Fluid Dyn. Res.*, **47**, 015506 (2015).
19. J. L. Beck, *Phys. Fluids*, **15**, 1377 (1972).
20. T. J. Chung, C. K. Choi, D.-Y. Yoon and M. C. Kim, *Int. J. Heat Mass Transfer*, **53**, 5139 (2010).
21. D. A. Nield and A. Bejan, *Convection in porous media*, 4th Ed., Springer, N.Y. (2013).
22. J. C. Ward, *J. Hydraul. Div.*, **90**, 1 (1964).
23. D. D. Joseph, D. A. Nield and G. Papanicolaou, *Water Resour. Res.*, **18**, 1049 (1982).
24. M. Kaviany, *Principle of heat transfer in porous media*, 2nd Ed., Springer, N.Y. (1995).
25. M. C. Kim, *Adv. Water Res.*, **35**, 1 (2012).

26. W. S. Ryoo and M. C. Kim, *Korean J. Chem. Eng.*, **35**, 1423 (2018).
27. M. C. Kim and C. K. Choi, *Korean J. Chem. Eng.*, **32**, 2400 (2015).
28. M. C. Kim, *Korean J. Chem. Eng.*, **38**, 144 (2021).
29. M. C. Kim, *Korean Chem. Eng. Res.*, **59**, 138 (2021).
30. X. Meng and Z. Guo, *Int. J. Heat Mass Transfer*, **100**, 767 (2016).
31. M. C. Kim, *Chem. Eng. Sci.*, **126**, 349 (2015).
32. M. C. Kim and Y. H. Kim, *Chem. Eng. Sci.*, **134**, 632 (2015).
33. J. T. H. Adress and S. S. S. Cardsso, *Chaos*, **22**, 037113 (2012).
34. T. K. Perkins, O. C. Johnston and R. N. Hoffman, *Soc. Pet. Eng. J.*, **5**, 301 (1965).

APPENDIX

By solving Eqs. (32) abd (33), can be obtained analytically by solving

$$\phi_i=\frac{l^*}{2}\left\{\exp(l^*\xi)\int_{\xi}^{\infty}\exp(-l^*\zeta)\mathrm{H}_i\left(\frac{\zeta}{2}\right)\exp\left(-\frac{\zeta^2}{4}\right)\mathrm{d}\zeta + \exp(-l^*\xi)\int_{-\infty}^{\xi}\exp(l^*\zeta)\mathrm{H}_i\left(\frac{\zeta}{2}\right)\exp\left(-\frac{\zeta^2}{4}\right)\mathrm{d}\zeta\right\}, \tag{A1}$$

By following Kim and Choi's [27] approach, Eq. (A1) can be expressed as

$$\psi_n=4l^{*2}(\psi_{n-2}+\phi_{n-2}),\ \mathrm{n}=2,\ 3,\ 4\cdots, \tag{A2}$$

with

$$\psi_0=-\frac{l^*}{2}\sqrt{\pi}\exp(l^{*2})\left[\exp(l^*\zeta)\mathrm{erfc}\left(\frac{\zeta}{2}+l^*\right)+\exp(l^*\zeta)\left\{1+\mathrm{erf}\left(\frac{\zeta}{2}-l^*\right)\right\}\right], \tag{A3}$$

and

$$\psi_1=l^*\exp(l^{*2})\left[\exp(l^*\zeta)\left\{\exp\left(-\left(\frac{\zeta}{2}+l^*\right)^2\right)-l^*\sqrt{\pi}\,\mathrm{erfc}\left(\frac{\zeta}{2}+l^*\right)\right\} + \exp(-l^*\zeta)\left\{\exp\left(-\left(\frac{\zeta}{2}-l^*\right)^2\right)-l^*\sqrt{\pi}\left(1+\mathrm{erf}\left(\frac{\zeta}{2}-l^*\right)\right)\right\}\right]. \tag{A4}$$